

Journal of Biomedical Optics

SPIEDigitalLibrary.org/jbo

Determination of optical absorption coefficient with focusing photoacoustic imaging

Zhifang Li
Hui Li
Zhiping Zeng
Wenming Xie
Wei R. Chen

Determination of optical absorption coefficient with focusing photoacoustic imaging

Zhifang Li,^a Hui Li,^a Zhiping Zeng,^a Wenming Xie,^a and Wei R. Chen^b

^aFujian Normal University, School of Physics and OptoElectronics Technology, Fujian Provincial Key Laboratory of Photonic Technology, Key Laboratory of Optoelectronic Science and Technology for Medicine, Ministry of Education, Fuzhou, Fujian 350007, China

^bUniversity of Central Oklahoma, Department of Engineering and Physics, Edmond, Oklahoma 73034

Abstract. Absorption coefficient of biological tissue is an important factor for photothermal therapy and photoacoustic imaging. However, its determination remains a challenge. In this paper, we propose a method using focusing photoacoustic imaging technique to quantify the target optical absorption coefficient. It utilizes the ratio of the amplitude of the peak signal from the top boundary of the target to that from the bottom boundary based on wavelet transform. This method is self-calibrating. Factors, such as absolute optical fluence, ultrasound parameters, and Grüneisen parameter, can be canceled by dividing the amplitudes of the two peaks. To demonstrate this method, we quantified the optical absorption coefficient of a target with various concentrations of an absorbing dye. This method is particularly useful to provide accurate absorption coefficient for predicting the outcomes of photothermal interaction for cancer treatment with absorption enhancement. © 2012 Society of Photo-Optical Instrumentation Engineers (SPIE). DOI: 10.1117/1.JBO.17.6.061216]

Keywords: photoacoustic imaging; absorption coefficient; wavelet transform; photothermal effects.

Paper 11468SS received Aug. 30, 2011; revised manuscript received Feb. 12, 2012; accepted for publication Feb. 27, 2012; published online May 21, 2012.

1 Introduction

Photoacoustic (PA) imaging can provide images proportional to the distribution of the absorbed optical energy density. It has already demonstrated its ability to detect breast cancer, skin related diseases, and brain tumors in small-animal studies.¹⁻⁵ Generation of photoacoustic signals can be classified according to two excitation modes: continuous-wave modulation and pulsed mode. The shape of the time-resolved photoacoustic signal depends on the physical characteristics of the irradiated body and the properties of the optical exciting pulse.^{6,7}

It is well known that the temporal amplitude and profile of photoacoustic signals are spatial mappings of the absorbed optical energy, which is the product of the optical absorption coefficient μ_a and the fluence $F(r)$. The local laser fluence $F(r)$ at the absorber is determined by a combination of optical absorption and optical scattering of background medium. Considerable attention has been devoted to methods for extracting the tissue optical absorption coefficient μ_a from the detected photoacoustic signals. Currently, these methods may be divided into two categories. One is based on the temporal profiles of photoacoustic signal combined with a light transport model.⁸⁻¹⁶ The other involves solving the photoacoustic wave equation and frequency-domain coupled with photon diffusion equation with iterative algorithms.¹⁷⁻²⁰

Spectra of photoacoustic signals are also used to quantify optical absorption coefficients.²¹ This method is calibration-free since it deals only with the relative change in various acoustic frequencies. However, this method uses two optical wavelengths and ignores the wavelength-dependent fluence.

In this paper, we present a model for determining the optical absorption coefficient of a heterogeneous absorber using photoacoustic imaging. In this model, the ratio of the amplitude of the peak signal from the top boundary to that from the bottom boundary (TBR) of the absorbing sample is an exponential function of the absorption coefficient. The theoretical component of this method can demonstrate that the optical absorption coefficient could be recovered using TBR. This method is self-calibrating, since it depends only on the relative change of the peak signals from both the top and bottom boundaries of the absorbing target. In addition, we performed experiments to validate this model based on wavelet transform. Finally, the method is applied to determine the absorption coefficient of an absorber with different concentrations of ink.

2 Theory and Methods

2.1 Photoacoustic Signal Generation and Detection

The photoacoustic measurement geometry used in this study is depicted in Fig. 1. Photoacoustic signals are generated in the phantom experiment by irradiating the surface with nanosecond pulses of NIR laser light. The absorption of the optical energy leads to near-impulsive heating of the irradiated volume followed by rapid thermoelastic expansion. The photoacoustic pressure is governed by the following wave equation:

$$\nabla^2 p(\vec{r}, t) - \frac{1}{c^2} \frac{\partial^2 p(\vec{r}, t)}{\partial t^2} = \frac{-\beta \partial \Phi(\vec{r}, t)}{C_p \partial t}, \quad (1)$$

where p is the wave pressure, $\vec{r} = (x, y, z)$ denotes the position, t is the time, c is the speed of the acoustic wave in the medium, β is the thermal expansion coefficient, C_p is the constant pressure

Address all correspondence to: Hui Li, Fujian Normal University, School of Physics and OptoElectronics Technology, Fujian Provincial Key Laboratory of Photonic Technology, Key Laboratory of Optoelectronic Science and Technology for Medicine, Ministry of Education, Fuzhou, Fujian 350007, China. E-mail: hli@fjnu.edu.cn; Wei R. Chen, University of Central Oklahoma, Department of Engineering and Physics, Edmond, Oklahoma 73034, E-mail: wchen@uco.edu

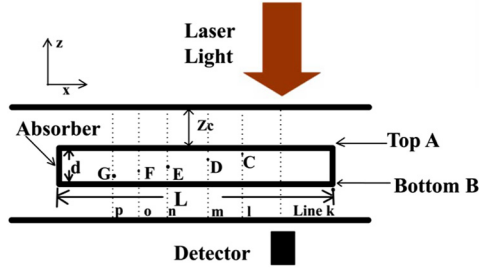


Fig. 1 Cross-sectional schematic of photoacoustic imaging with focused transducer. The phantom is made of Agar gel with a cylindrical target (length l and diameter d) with a distance of z_c from the surface of the phantom. The scanning of the exciting laser beam is from left to right with several typical A-lines labeled as lines k , l , m , n , o , and p . Lead-pencil absorbers are placed at C , D , E , F , and G .

specific heat capacity, and Φ is the absorbed optical energy density. When the laser pulse is sufficiently short, the optical energy density Φ can be modeled as a δ function in time,

$$\Phi(\vec{r}, t) = \Phi(\vec{r})\delta(t). \quad (2)$$

The optical energy density $\Phi(\vec{r})$ is a product of optical absorption coefficient $\mu_a(\vec{r})$ and optical fluence $F(\vec{r})$,

$$\Phi(\vec{r}) = \mu_a(\vec{r})F(\vec{r}). \quad (3)$$

The initial acoustic pressure $p(\vec{r})$ is proportional to the absorbed energy density $\Phi(\vec{r})$,

$$p(\vec{r}) = K\Phi(\vec{r}), \quad (4)$$

where K is a proportionality coefficient related to the ultrasonic parameters, the Grüneisen parameter, and the efficiency of the conversion of heat to pressure. Since the photoacoustic signals usually involve a wide range of frequencies, $p(\vec{r})$ could be expressed as the sum of signals at different acoustic frequencies f : $p(\vec{r}) = \sum p(\vec{r}, f)$.

The measured photoacoustic signal $S(\vec{r})$ should be the convolution of $p(\vec{r})$ with the detector geometry,²² given by $S(\vec{r}) = \sum S(\vec{r}, f)$. The two common computational challenges for photoacoustic imaging are directional sensitivity of the detector and acoustic attenuation during the geometric spreading of the propagating wavefronts.²³ To circumvent the two challenges, we used a focusing transducer featuring extended focal zone, which is much larger than the dimensions of the signal source. We also used the following approximation,²⁴

$$p(\vec{r}) = \sum p(\vec{r}, f) = \sum S(\vec{r}, f) \exp(\alpha_f D_{st}), \quad (5)$$

for correcting initial acoustic amplitude $p(\vec{r})$ from measured signal $S(\vec{r})$, where α_f is the attenuation coefficient dependent on the frequency, and D_{st} is the distance between the photoacoustic signal source and detector. In Eq. (5), the attenuation coefficient α_f satisfies a power law dependence on frequency: $\alpha_f = \alpha_{0f}|f|^n$, where n is a real positive constant, α_{0f} is the attenuation constant, and f is the acoustic frequency. For many biological tissues, $n \approx 1$, and the average attenuation coefficient is $\alpha_{0f} \approx 0.5 \text{ dB} \cdot \text{MHz}^{-1} \cdot \text{cm}^{-1}$.²⁴

2.2 Recovering Optical Absorption Coefficient

As can be seen from Eq. (4), the explicit expression of the absorbed energy density $\Phi(\vec{r})$ is important for the description of the photoacoustic signal. We employ a simple phantom with a pure absorber (with an optical absorption coefficient $\Delta\mu_a$) embedded in a homogeneous scattering medium (with scattering coefficient μ_s , absorption coefficient μ_a , and the anisotropy g). The distance between the absorber and the surface of medium is z_c , as shown in Fig. 1. If we use F_0 to denote the incident fluence on the surface of the absorber, the fluence inside the absorber obeys Beer's law:

$$p(z) = K\Delta\mu_a F_0 \exp(-\Delta\mu_a z).$$

F_0 is determined by a combination of optical absorption and optical scattering of the intervening medium between the phantom surface and the absorber. For simplicity, we assumed a low scattering coefficient for the background medium in the theoretical calculation. In the background scattering region, F_0 is given by:

$$F_0 \propto \exp[-(\mu_s + \mu_a)z_c]. \quad (6)$$

Thus the photoacoustic pressure can be expressed as:

$$p \propto K\Delta\mu_a \exp[-(\mu_s + \mu_a)z_c] \exp(-\Delta\mu_a z). \quad (7)$$

Since the photoacoustic method directly measures the effective fluence at an absorber located inside the tissue, Eq. (7) implies that fitting the amplitude of photoacoustic signal versus the depth of the absorbing medium leads to the recovery of the absorption coefficient of the target.

Since the photoacoustic method is sensitive to boundaries of strong absorbing media,²⁵ we focus on the properties of photoacoustic signals from the top and bottom boundaries of the target. At the top of the absorber, $z = 0$, Eq. (7) can be simplified as:

$$p_1 \propto K\Delta\mu_a \exp[-(\mu_s + \mu_a)z_c]. \quad (8)$$

At the bottom of the absorber $z = d$, Eq. (7) can be obtained by:

$$p_2 \propto K\Delta\mu_a \exp[-(\mu_s + \mu_a)z_c] \exp[-\Delta\mu_a d]. \quad (9)$$

By simply dividing the photoacoustic amplitudes measured at the top and bottom boundaries of the target, we can eliminate the effects of the depth z_c and the ultrasonic parameters. The TBR of the target, obtained by Eq. (9) divided by Eq. (8), can be expressed as

$$\text{TBR} = p_2/p_1 = \exp[-\Delta\mu_a d]. \quad (10)$$

Equation (10) shows that the TBR is independent of the proportionality coefficient K and the optical properties (μ_a and μ_s) of the background medium and the target depth z_c . Then the absorption coefficient of the target can be determined by

$$\Delta\mu_a = -\ln(p_2/p_1)/d. \quad (11)$$

The size d of absorber was determined by multiplying the time interval Δt with the speed c of sound in the medium. Thus the optical absorption coefficient $\Delta\mu_a$ can be written in term of the time interval Δt as:

$$\Delta\mu_a = -\ln(p_2/p_1)/(c\Delta t). \quad (12)$$

The velocity c of ultrasonic wave in the medium is approximately 1.5 mm/ μ s.

2.3 Experimental Setup

The photoacoustic system used for this study is described in detail in our previous publication.²⁶ Instead of backward-detection mode, the forward-detection mode was employed, as shown in Fig. 1. In this system, a pulse light from a Nd:YAG laser (beam diameter \sim 1.5 cm, wavelength: 830 nm, pulse duration: 6 ns) was used to irradiate the phantom to generate an acoustic pressure wave. One-dimensional, depth-resolved photoacoustic signals (A-scan) were collected by scanning with a wide-bandwidth focused transducer (frequencies from 1 to 7 MHz). In order to improve the signal-to-noise ratio, we used 512 series of pulses and obtained the average signal. The scanning was performed by moving the sample through computer-controlled step-motors along x -axis. The axial and lateral spatial resolutions of the photoacoustic imaging are 0.3 and 2 mm, respectively.

For all the experiments, the phantom was made of Agar gel with Intralipid as scatterers and ink as absorbers. The homogeneous background contained 2 g Agar power, 2-ml Intralipid-20% solution (Sino-Swed Pharmaceutical Corp. Ltd), and 100 ml distilled water. The background optical scattering coefficient was approximately 8.2 cm^{-1} at the wavelength of 830 nm (Ref. 27), which satisfies the condition of single scattering. The background absorption coefficient can be neglected. The cylindrical absorbing target was made of Agar gel (2-g Agar power and 50-ml distilled water) with different volume of ink (1, 0.5, 0.33, 0.25, 0.2 or 0.05 ml). The length L and the diameter d of absorbing target are 5 and 6 mm, respectively.

2.4 Wavelet Transform

Since this model only depends on the peak information of the signals from the boundaries of the absorber, we need to extract the envelope of these peaks, rather than the profile of photoacoustic signals. The acoustic signals usually involve a wide range of frequencies, typically from 50 Hz to 50 MHz. Furthermore, the acoustic attenuation is dependent on the frequency.²⁴ In order to restore the amplitude of photoacoustic signal after

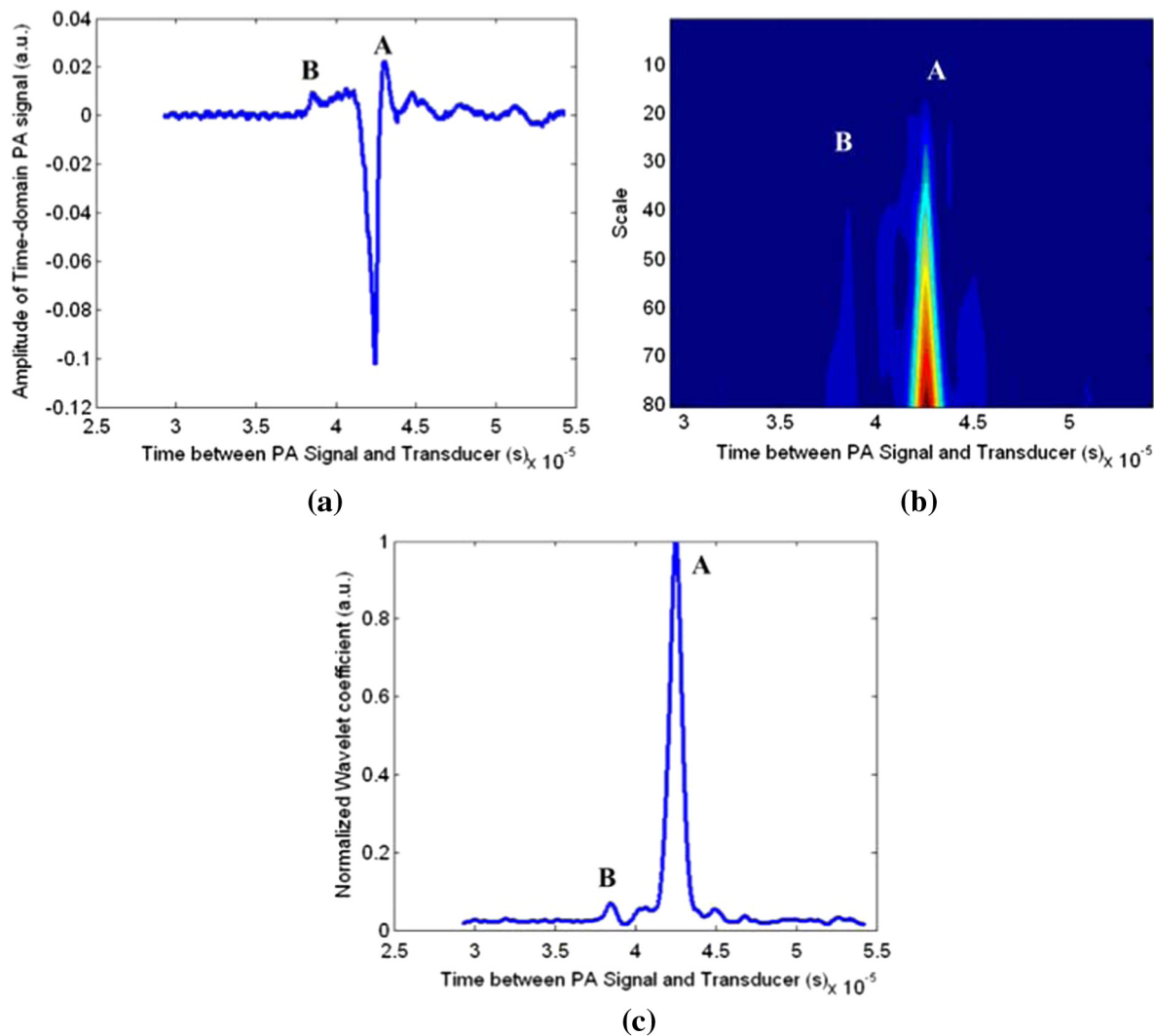


Fig. 2 PA signal and wavelet transform of a typical photoacoustic A-line (line k in Fig. 1): (a) raw data; (b) the corresponding wavelet coefficients; (c) superposition of wavelet coefficients from scales 16 to 80. A and B denote the positions of the top and the bottom of the ink block, respectively.

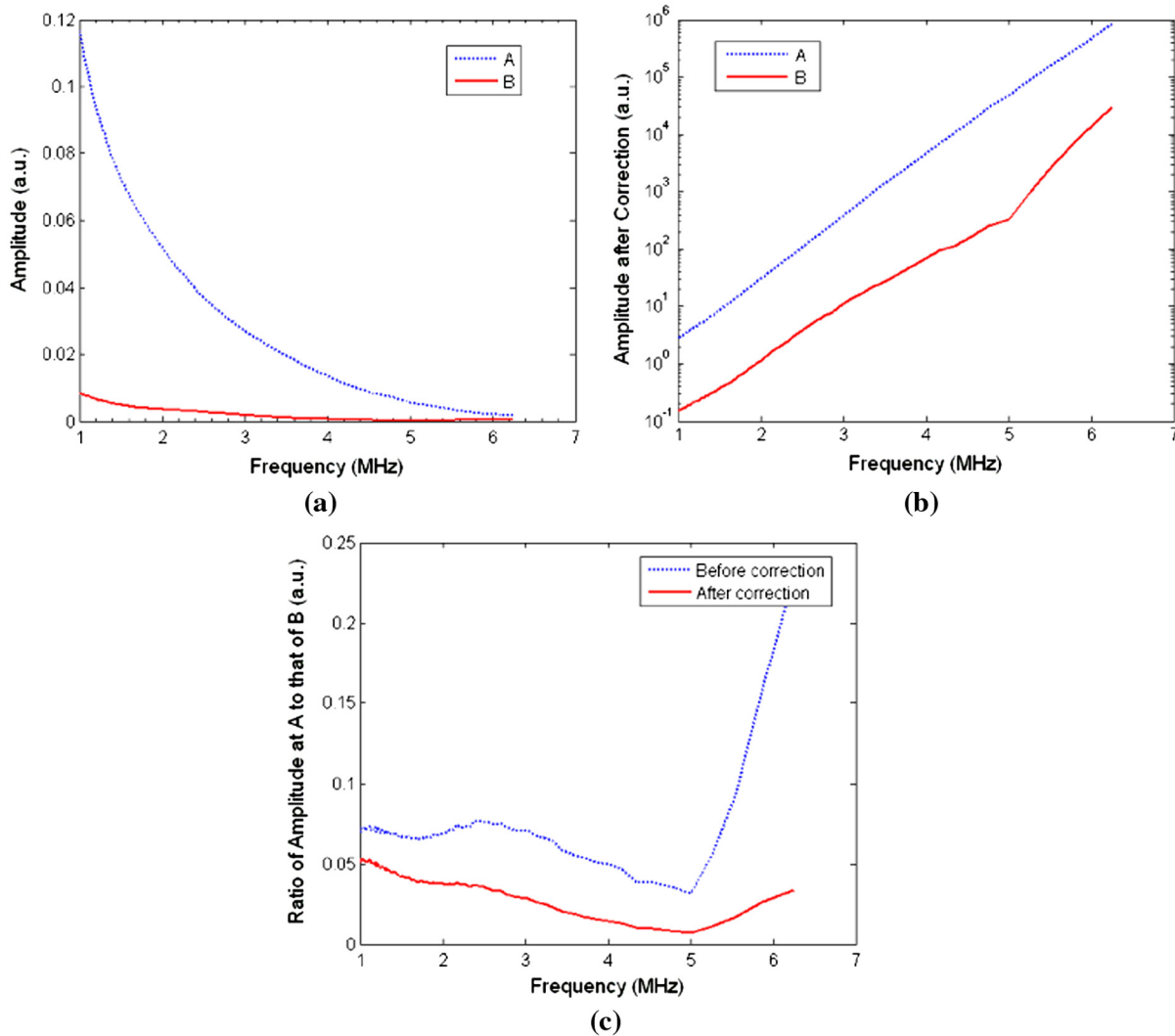


Fig. 3 Wavelet coefficients versus acoustic frequencies at top and bottom boundaries of the sample before correction (a), after correction (b), and the ratio of wavelet coefficient of the top boundary to that of the bottom boundary (c).

propagation, we decided to use wavelet transform to extract the photoacoustic signals at specific acoustic frequencies and correct them using Eq. (5).

The wavelet transform is an effective method to extract the envelope of a temporal photoacoustic signal at various frequencies. Then the frequency dependence of acoustic attenuation is applied to restore the amplitude of peak signal based on Eq. (5). Furthermore, the wavelet transform can improve the signal-to-noise (SNR). Since the photoacoustic signal is higher than the noise in some specific frequency band, the superposition of the photoacoustic signals in the specific frequency band further improves the SNR.

In this work, the continuous wavelet transform (CWT) is employed for analyzing the photoacoustic signals:²⁶

$$\text{CWT}(a, b) = \frac{1}{\sqrt{a}} \int S(t) \Psi\left(\frac{t-b}{a}\right) dt, \quad (13)$$

where $S(t)$ represents the detected photoacoustic signal, t is the arrival time of the photoacoustic signal, CWT denotes the continuous wavelet transform, a is the scale parameter related to the

frequency, and b denotes the time shift parameter. In this study, the complex Morlet wavelet is used.

3 Results

Figure 2(a) and 2(b) shows the typical A-line photoacoustic signals and the corresponding wavelet transform. Figure 2(a) shows the bipolar nature of the temporal photoacoustic signals from the top surface of the target. The signals from the bottom surface appear to be monopolar simply because they are weak and are buried in the tails of top surface signals. Result in Fig. 2(b) indicates that the wavelet coefficient below scale 16 is approximately homogeneous due to noise, and the wavelet coefficient of the photoacoustic signal increases from scales 16 to 80. The Fourier frequencies corresponding with the scales from 16 to 80 are from 6.25 MHz to 1 MHz. The wide-bandwidth-focused transducer is sensitive to the frequency in this range. In order to improve the signal-to-noise ratio (SNR), the superposition of wavelet coefficients from scales 16 and 80 is used, as shown in Fig. 2(c). The maximal values in Fig. 2(c) indicate the locations of the boundaries of the target (A and B). The size of the absorber is calculated by multiplying

the time interval between A and B with the speed of sound in the medium.

Since the acoustic attenuation coefficient depends on the frequency, the measured peak photoacoustic signals at both boundaries are chosen from the wavelet transform, as shown in Fig. 3(a). According to Eq. (5), the data in Fig. 3(a) are corrected, and the results are shown in Fig. 3(b). Results in Fig. 3(c) demonstrate that the frequency dependence of the profile and amplitude of the ratio of wavelet coefficient of the top boundary to that of the bottom boundary is different after correction.

The peak values of wavelet coefficient of pencil leads (C, D, E, F, and G), as shown in Fig. 1, were used to extract the absorption coefficient based on Eq. (7). Figure 4 shows the plot of the peak values of wavelet coefficients after the correction using Eq. (5) versus the depth of the absorber. For a target with 0.1% ink, the $\Delta\mu_a$ was determined as $2.7 \pm 0.2 \text{ cm}^{-1}$ based on Eq. (7). In comparison, using the restored amplitudes at the top and bottom boundaries (A and B as shown in Fig. 1), we obtained an absorption coefficient of $2.9 \pm 0.3 \text{ cm}^{-1}$ based on Eq. (11). These results validated our proposed method using TBR of the target.

With the corrections for the attenuation of the peak amplitudes at the top and bottom boundaries using Eq. (5), we obtained absorption coefficients of samples based on Eq. (11). The absorption coefficients of six samples with different concentrations (0.1 to 2%) of ink are given in Fig. 5. The absorption coefficients obtained using our new method ranged from 2.9 to 5.6 cm^{-1} , linearly related to the concentration of the ink from 0.1 to 1%. However, at the highest concentration (2%), the absorption coefficient is noticeably lower below the linear fit, which may be explained by nonlinear optical absorption coefficient.²⁸

4 Discussion

Since biological tissues are strong scattering media, diffusion approximation of local fluence rate should be used for characterizing the optical properties. In the diffusive region, the light fluence along the axial direction is reduced due to absorption and scattering.¹⁵ The fluence can be expressed as $F_0 = C_0 \exp(-\mu_{\text{eff}}z)$, where C_0 is a constant, and

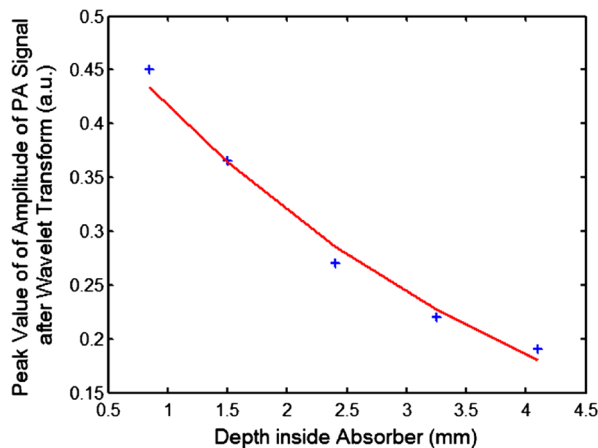


Fig. 4 The peak values of wavelet coefficient of different pencil leads as a function of depths inside the target, after signal correction using Eq. (5). The fitting curve is used to determine the absorption coefficient of the target using Eq. (7).

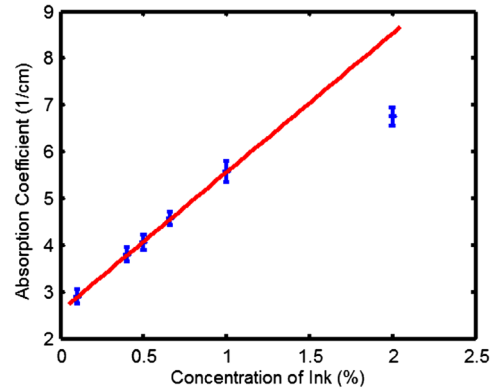


Fig. 5 Absorption coefficients of absorbers with different concentrations of ink. Data represent mean \pm standard deviation ($n = 10$).

$\mu_{\text{eff}} = 3\mu_a[\mu_a + \mu_s(1 - g)]$. Since our method for determining absorption coefficient of target using the TBR depends on the incident fluence on the surface, it can be used for strong scattering background medium. Moreover, the scattering coefficient and the anisotropy of highly scattering medium can be determined by optical coherence tomography (OCT).²⁹ Thus we could combine the photoacoustic imaging and OCT for simultaneous determination of absorption coefficient of heterogeneous absorbers and the optical scattering properties of the background.

Our method is self-calibrating, since it deals only with the relative change in the signals from the top and bottom boundaries of the absorbing target. In addition, this method uses different wavelengths of laser light to study the wavelength-dependent absorption property of targets.

Tissue absorption coefficient is an important factor in imaging and therapy based on photothermal interactions. Different methods have been used to determine the absorption coefficients of different target tissues. Yet a reliable accurate method is still not available. This study proposes a novel method to noninvasively determine absorption coefficient using photoacoustic method. This method is particularly useful in determining the outcomes of selective photothermal interaction for cancer treatment with absorption enhancement of target tumors using either chemical dye^{30–32} or nanoparticles.³³ Using accurate absorption coefficients, simulations of photothermal effects^{34,35} can yield more reliable predictions for laser irradiation of biological tissues.

5 Conclusions

In summary, we demonstrated the feasibility of a new method using TBR of absorbing target to quantify the optical absorption coefficient with a focusing photoacoustic imaging technique based on the wavelet transform. The wavelet transform is used to locate the boundaries of the target and to extract photoacoustic signals at the specific ultrasound frequency. The theoretical analysis reveals that the TBR is an exponential function of the absorption coefficient of a heterogeneous absorber and is independent of absolute optical fluence, the ultrasound parameters, and the Grüneisen parameter. Our method was validated experimentally using an ink-enhanced absorbing target buried in a low-scattering medium. This method could be beneficial to absorption-based imaging and therapy by providing an accurate absorption coefficient.

Acknowledgments

This project was sponsored in part by Fujian Provincial Key Program of Science and Technology under No. 2011Y0019, National Natural Science Foundation of China under No. 61178089, Fujian Provincial Natural Science Foundation under No. 2011J01005, the Research Fund for the Doctoral Program of Higher Education under No. 200803940001, and by Fujian Provincial Education Scientific Project under No. JA11057. The author (Wei R. Chen) would like to acknowledge the support of a US Fulbright scholarship for the 2011 to 2012 academic year.

References

1. M. Xu and L. V. Wang, "Photoacoustic imaging in biomedicine," *Rev. Sci. Instrum.* **77**(4), 041101 (2006).
2. X. Xu and H. Li, "Photoacoustic imaging in biomedicine," *Physics* **37**(2), 111–119 (2008) (In Chinese).http://159.226.36.45/jwk_wl/CN/abstract/abstract31161.shtml
3. C. Li and L. V. Wang, "Photoacoustic tomography and sensing in biomedicine," *Phys. Med. Biol.* **54**(19), R59–R97 (2009).
4. J. Gamelin et al., "Curved array photoacoustic tomographic system for small animal imaging," *J. Biomed. Opt.* **13**(2), 024007 (2008).
5. S. A. Ermilov et al., "Laser optoacoustic imaging system for detection of breast cancer," *J. Biomed. Opt.* **14**(2), 024007 (2009).
6. C. G. A. Hoelen and F. F. M. de Mul, "A new theoretical approach to photoacoustic signal generation," *J. Acoust. Soc. Am.* **106**(2), 695–706 (1999).
7. G. J. Diebold, T. Sun, and M. I. Khan, "Photoacoustic monopole radiation in one, two, and three dimensions," *Phys. Rev. Lett.* **67**(24), 3384–3387 (1991).
8. Y. Wang and R. Wang, "Photoacoustic recovery of an absolute optical absorption coefficient with an exact solution of a wave equation," *Phys. Med. Biol.* **53**(21), 6167–6177 (2008).
9. A. A. Oraevsky, S. L. Jacques, and F. K. Tittel, "Measurement of tissue optical properties by time-resolved detection of laser-induced transient stress," *Appl. Opt.* **36**(1), 402–415 (1997).
10. W. Xie et al., "Measurement of optical properties of biological tissue based on scanning photoacoustic technology," *Laser Optoelect. Prog.* **46**(12), 103–107 (2009) (in Chinese)
11. B. T. Cox et al., "Quantitative photoacoustic imaging: fitting a model of light transport to the initial pressure distribution," *Proc. SPIE* **5697**, 49–55 (2005).
12. B. T. Cox et al., "Two-dimensional quantitative photoacoustic image reconstruction of absorption distributions in scattering media by use of a simple iterative method," *Appl. Opt.* **45**(8), 1866–1875 (2006).
13. J. C. Ranasinghesagara et al., "Photoacoustic technique for assessing optical scattering properties of turbid media," *J. Biomed. Opt.* **14**(4), 040504 (2009).
14. R. O. Esenaliev et al., "Optoacoustic technique for noninvasive monitoring of blood oxygenation: a feasibility study," *Appl. Opt.* **41**(22), 4722–4731 (2002).
15. J. Laufer et al., "In vitro measurements of absolute blood oxygen saturation using pulsed near-infrared photoacoustic spectroscopy: accuracy and resolution," *Phys. Med. Biol.* **50**(18), 4409–4428 (2005).
16. Y. Y. Petrov et al., "Multiwavelength optoacoustic system for noninvasive monitoring of cerebral venous oxygenation: a pilot clinical test in the internal jugular vein," *Opt. Lett.* **31**(12), 1827–1829 (2006).
17. Z. Yuan and H. Jiang, "Quantitative photoacoustic tomography: recovery of optical absorption coefficient maps of heterogeneous media," *Appl. Phys. Lett.* **88**(23), 231101 (2006).
18. Z. Yuan, Q. Zhang, and H. Jiang, "Simultaneous reconstruction of acoustic and optical properties of heterogeneous media by quantitative photoacoustic tomography," *Opt. Express* **14**(15), 6749–6754 (2006).
19. Z. Yuan, Q. Wang, and H. Jiang, "Reconstruction of optical absorption coefficient maps of heterogeneous media by photoacoustic tomography coupled with diffusion equation based regularized Newton method," *Opt. Express* **15**(26), 18076–18081 (2007).
20. Z. Yuan and J. Jiang, "Quantitative photoacoustic tomography," *Philos. Trans. A Math. Phys. Eng. Sci.* **367**(1900), 3043–3054 (2009).
21. Z. Guo, S. Hu, and L. V. Wang, "Calibration-free absolute quantification of optical absorption coefficients using acoustic spectra in three-dimensional photoacoustic microscopy of biological tissue," *Opt. Lett.* **35**(12), 2067–2069 (2010).
22. K. P. Kostli and P. C. Beard, "Two-dimensional photoacoustic imaging by use of Fourier-transform image reconstruction and a detector with an anisotropic response," *Appl. Opt.* **42**(10), 1899–1908 (2003).
23. J. Laufer et al., "Quantitative spatially resolved measurement of tissue chromophore concentrations using photoacoustic spectroscopy," *Phys. Med. Biol.* **52**(1), 141–168 (2007).
24. X. L. Dean-Ben, D. Razansky, and V. Ntziachristos, "Correction for acoustic attenuation effects in optoacoustic tomographic reconstructions," *Proc. of SPIE* **8090**, 809014 (2011).
25. Z. Guo, L. Li, and L. V. Wang, "On the speckle-free nature of photoacoustic tomography," *Med. Phys.* **36**(9), 4084–4088 (2009).
26. Z. Li et al., "In vivo determination of acute myocardial ischemia based on photoacoustic imaging with a focused transducer," *J. Biomed. Opt.* **16**(7), 076011 (2011).
27. H. J. van Staveren et al., "Light scattering in Intralipid-10% in the wavelength range of 400–1100 nm," *Appl. Opt.* **30**(31), 4507–4514 (1991).
28. C. S. Yelleswarapu and S. R. Kothapalli, "Nonlinear photoacoustics for measuring the nonlinear optical absorption coefficient," *Opt. Express* **18**(9), 9020–9025 (2010).
29. V. M. Kodach et al., "Determination of the scattering anisotropy with optical coherence tomography," *Opt. Express* **19**(7), 6131–6140 (2011).
30. W. R. Chen et al., "Chromophore-enhanced laser-tumor tissue photothermal interaction using 808 nm diode laser," *Cancer Lett.* **88**(1), 15–19 (1995).
31. W. R. Chen et al., "Chromophore-enhanced in vivo tumor cell destruction using an 808-nm diode laser," *Cancer Lett.* **94**(2), 125–131 (1995).
32. W. R. Chen et al., "Photothermal effects on murine mammary tumors using indocyanine green and an 808-nm diode laser: An in vivo efficacy study," *Cancer Lett.* **98**(2), 169–173 (1996).
33. L. R. Hirsch et al., "Nanoshell-mediated near-infrared thermal therapy of tumors under magnetic resonance guidance," *Proc. Natl. Acad. Sci. USA* **100**(23), 13549–13554 (2003).
34. L. V. Wang, R. E. Nordquist, and W. R. Chen, "Optimal beam size for light delivery to absorption-enhanced tumors buried in biological tissues and effect of multiple beam delivery: a Monte Carlo study," *Appl. Opt.* **36**(31), 8286–8291 (1997).
35. J. J. Crochet et al., "Temperature distribution in selective laser-tissue interaction," *J. Biomed. Opt.* **11**(3), 034031 (2006).